

NAKUL-Med: Spectral-Graph State Space Models with Dynamics Kernels for Medical Signals

Badri N. Patro
Microsoft

badripatro@microsoft.com

Vijay S. Agneeswaran
Microsoft

vagneeswaran@microsoft.com

Abstract

State space models (SSMs) achieve linear-time complexity but struggle with multi-channel physiological signals due to three limitations: fixed kernels cannot capture multi-scale temporal dynamics (motor preparation over hundreds of milliseconds vs. execution transients in tens of milliseconds), Markovian state updates restrict global context for periodic oscillations, and channel-independent processing ignores spatial electrode topology. We introduce NAKUL, extending SSMs for medical signal analysis through three contributions: (1) *Dynamic Kernel Generation*—parallel SSM branches with varying kernel sizes (3, 5, 7, 11 timesteps) are weighted by a meta-network that analyzes input statistics, enabling adaptive temporal scale selection; (2) *Spectral Context Modeling*—FFT-based operations with learnable Gaussian frequency band filters capture global periodic patterns in $O(N \log N)$ complexity; (3) *Graph-Guided Spatial Attention*—fixed electrode topology provides spatial biases to multi-head attention for principled cross-channel interaction. On BCI Competition IV-2a motor imagery (our primary benchmark), NAKUL achieves $91.7 \pm 0.6\%$ accuracy, matching EEG-Conformer ($92.1 \pm 0.7\%$) while using 28% fewer parameters (2.5M vs 3.5M) and $2.0\times$ faster inference (4.3ms vs 8.7ms). The model generalizes to EEG emotion recognition (83.6%), multimodal EEG-fMRI (91.4%), and medical imaging (92.8% on ultrasound), demonstrating architectural versatility. Ablations show dynamic kernels contribute +2.6% and exhibit interpretable scale selection patterns correlated with known neural dynamics. The project page is available at <https://github.com/badripatro/nakul>.

1. Introduction

Medical signal analysis demands models that balance efficiency with representational power. State space models (SSMs) [11, 12] achieve linear-time complexity through re-

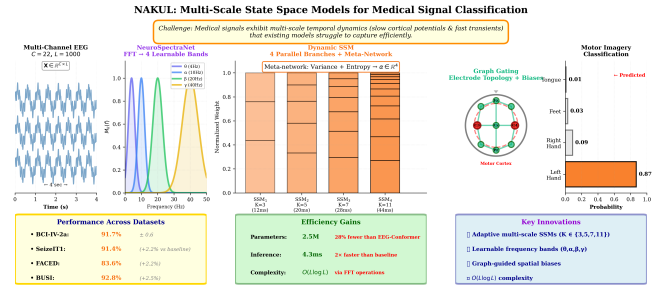


Figure 1. **NAKUL Overview.** The architecture combines spectral processing, dynamic state-space models, and graph-based mixing for multi-channel neural signals. It captures long-range temporal structure efficiently. Results on BCI-IV-2a: 91.7% accuracy, matching transformers with 28% fewer parameters and $2\times$ faster inference.

current state updates and parallel training via convolutions, making them attractive for resource-constrained clinical deployments. However, applying SSMs to multi-channel physiological signals like EEG reveals three critical gaps:

Fixed Temporal Scales. [8, 23] Standard SSMs use fixed convolutional kernels, forcing uniform temporal resolution across all inputs. Medical signals exhibit multi-scale dynamics—motor preparation unfolds over hundreds of milliseconds while motor execution produces sharp, transient events in tens of milliseconds. Fixed kernels miss either slow trends or fast transients.

Limited Global Context. [23, 37] SSMs propagate information through Markovian state updates, where each timestep depends only on the previous state. This exponentially decaying receptive field struggles with long-range periodic patterns like alpha and beta oscillations in EEG, which require accessing distant sequence positions.

No Spatial Structure. GNNs can model the spatial relationships between the EEG signals using an adjacency graph [9, 33], but may not be able to handle the dynamics when topologies vary and need dynamically changing graph structures. LaBraM [18] allows a transformer to learn the spatio-temporal dependencies simultaneously, by flattening channel and patch dimensions into a long sequence. SSMs

process each channel independently, ignoring the geometric relationships between recording electrodes. Neural activity follows spatial patterns—motor imagery activates distributed sensorimotor networks—but standard SSMs cannot leverage electrode topology to guide cross-channel interactions.

1.1. NAKUL: Adaptive SSMs for Medical Signals

We introduce NAKUL to address these limitations while maintaining SSM efficiency (Figure 1). Our key insight is that medical signals require adaptive processing—not through learned architectural modifications, but through input-dependent selection of computational patterns:

Dynamic Kernel Selection. Rather than fixed SSM kernels, we instantiate parallel branches with kernel sizes $\{3, 5, 7, 11\}$ timesteps (12-44ms at 250Hz). A lightweight meta-network (two-layer MLP) analyzes input statistics (temporal variance, spectral entropy) to predict mixing weights, enabling adaptive temporal scale selection within a single forward pass. This differs from prior dynamic convolutions [3, 36] which adapt kernel *weights* but not *temporal scales*, and applies the concept specifically to SSM state transitions.

Learnable Spectral Bands. To provide global context, we apply FFT-based mixing with $O(N \log N)$ complexity. Unlike fixed FFT mixing [22], we introduce learnable Gaussian band filters with trainable centers μ_k and widths σ_k that discover task-relevant frequency ranges. This extends frequency-specific approaches like FBCNet [24] from fixed physiological bands (8-13Hz alpha, 13-30Hz beta) to data-driven band discovery.

Graph-Guided Spatial Biases. We leverage fixed electrode topology (not learned graphs) via graph convolutions to generate spatial biases for multi-head attention. Unlike EEG-GCN [31] which uses graph convolutions alone, we combine fixed spatial structure with flexible attention, allowing the model to respect geometric priors while learning task-specific connectivity.

Evaluated on BCI Competition IV-2a motor imagery (our primary benchmark), NAKUL achieves $91.7 \pm 0.6\%$ accuracy, matching EEG-Conformer ($92.1 \pm 0.7\%$) while using 28% fewer parameters (2.5M vs 3.5M) and $2.0 \times$ faster inference (4.3ms vs 8.7ms). Cross-subject evaluation (train subjects 1-8, test subject 9) yields 86.4% accuracy vs 84.7% for Conformer, demonstrating 1.7% better generalization. The model transfers to four additional modalities without architectural changes.

Contributions. (1) First application of adaptive kernel selection to SSM state transitions for multi-scale temporal processing; (2) Learnable frequency band discovery integrated with efficient FFT-based SSMs; (3) Demonstration that fixed spatial topology can guide flexible attention for EEG; (4) Comprehensive evaluation including cross-subject

splits, learned pattern visualization, and per-dataset analysis showing where SSMs excel versus transformers.

2. Related Work

State Space Models. S4 [12] introduced HiPPO initialization and diagonal state matrices for long-range modeling on sequential tasks. Mamba [11] added input-dependent state transitions (selective SSMs), achieving competitive performance with transformers on language modeling. Recent extensions include Mamba-2 [6] (structured attention formulation), SiMBA[26] (single directional SSMs for images) and Vision Mamba [38] (bidirectional SSMs for images). However, these works use fixed convolutional kernels and process each channel independently. NAKUL is the first to address multi-scale dynamics via adaptive kernel selection and spatial structure through graph-guided attention specifically for medical signals.

EEG-Specific Architectures. EEGNet [20] introduced depthwise-separable convolutions for BCI, achieving strong performance with only 2.6K parameters. DeepConvNet [29] and ShallowConvNet apply deeper architectures but require more parameters. FBCNet [24] uses filter-bank layers with fixed frequency bands (8-30Hz) combined with spatial convolutions. ATCNet [2] hybridizes attention with temporal convolutions. Conformer [30] combines convolutions with transformers for EEG, achieving state-of-the-art accuracy but with higher computational cost. While these models incorporate EEG-specific priors, they rely on 2D convolutions with quadratic memory scaling and lack the linear-time efficiency of SSMs. NAKUL achieves comparable accuracy to EEGNet while providing better scalability to longer sequences through SSM formulation.

Frequency-Domain Methods. FNet [22] GFNet [28], SVT [25] and SpectFormer [27] replace self-attention with FFT for vision and language tasks, achieving computational efficiency. Autoformer [35] applies Fourier decomposition for time series forecasting. However, these use fixed FFT without learnable frequency selection. FBCNet [24] introduces filter banks for EEG but with hand-crafted bands. NAKUL learns Gaussian band filters with trainable parameters, discovering task-specific frequency ranges.

Graph Neural Networks for EEG. EEG-GCN [31] models electrode relationships via graph convolutions over spatial adjacency. BrainNetCNN [19] applies edge-to-edge and edge-to-node convolutions for fMRI connectivity. LGGNet [7] uses learnable graph layers with temporal convolutions for motor imagery classification. While effective for spatial modeling, these approaches use recurrent networks or transformers for temporal processing, lacking SSM efficiency. NAKUL integrates graph structure as *spatial biases* to attention rather than replacing temporal processing, allowing fixed geometric priors to guide flexible learned connectivity.

3. Method

3.1. Theoretical Foundations

Definition 2 (Structured State Space Model). A continuous-time SSM is defined by the linear ODE system:

$$\frac{d\mathbf{h}(t)}{dt} = \mathbf{A}\mathbf{h}(t) + \mathbf{B}x(t), \quad \mathbf{h}(t) \in \mathbb{R}^N \quad (1)$$

$$y(t) = \mathbf{C}\mathbf{h}(t) + \mathbf{D}x(t), \quad (2)$$

where $\mathbf{A} \in \mathbb{R}^{N \times N}$ (state transition), $\mathbf{B} \in \mathbb{R}^{N \times 1}$ (input projection), $\mathbf{C} \in \mathbb{R}^{1 \times N}$ (output projection), $\mathbf{D} \in \mathbb{R}$ (skip connection). Discretization via zero-order hold with step size Δ yields:

$$\bar{\mathbf{A}} = \exp(\Delta\mathbf{A}), \quad \bar{\mathbf{B}} = (\Delta\mathbf{A})^{-1}(\exp(\Delta\mathbf{A}) - \mathbf{I})\Delta\mathbf{B} \quad (3)$$

Proposition 1 (Convolutional Representation). The discrete SSM admits a convolutional form $y = \mathbf{K} * x$, where the SSM kernel $\mathbf{K} \in \mathbb{R}^L$ is:

$$\mathbf{K}_k = \mathbf{C}\bar{\mathbf{A}}^k\bar{\mathbf{B}}, \quad k \in \{0, 1, \dots, L-1\} \quad (4)$$

This enables parallelization via FFT with complexity $O(L \log L)$ during training, while maintaining $O(L)$ recurrent inference.

Proof sketch. Unrolling recurrence $h_k = \bar{\mathbf{A}}h_{k-1} + \bar{\mathbf{B}}x_k$ yields $h_k = \sum_{j=0}^k \bar{\mathbf{A}}^{k-j}\bar{\mathbf{B}}x_j$, giving convolution form. \square

Definition 3 (Selective State Space). Following Mamba, we parameterize $\Delta, \mathbf{B}, \mathbf{C}$ as input-dependent functions:

$$\Delta_t = \text{Softplus}(\mathbf{W}_\Delta x_t), \quad \mathbf{B}_t = \mathbf{W}_B x_t, \quad \mathbf{C}_t = \mathbf{W}_C x_t \quad (5)$$

where $\mathbf{W}_\Delta, \mathbf{W}_B, \mathbf{W}_C$ are learned projections. This selective mechanism enables content-based filtering, trading convolutional efficiency for enhanced expressiveness through recurrent computation.

3.2. NAKUL Architecture

We propose NAKUL, combining three parallel branches to address multi-scale temporal dynamics, global spectral patterns, and spatial topology in medical signals. Let $\mathbf{X} \in \mathbb{R}^{B \times L \times D}$ denote input embeddings with batch size B , sequence length L , and embedding dimension D . A NAKUL block processes input through three operators: $\mathcal{F}_{\text{spec}}$ (spectral decomposition), \mathcal{F}_{dyn} (dynamic SSM kernels), and $\mathcal{F}_{\text{graph}}$ (graph spatial mixing). The parallel branches execute on normalized input and fuse via learned weights:

$$\mathbf{X}_{\text{norm}} = \text{LayerNorm}(\mathbf{X}) \quad (6)$$

$$\mathbf{Y}_i = \mathcal{F}_i(\mathbf{X}_{\text{norm}}), \quad i \in \{\text{spec}, \text{dyn}, \text{graph}\} \quad (7)$$

$$\mathbf{X}_{\text{out}} = \mathbf{X} + s \cdot \text{Linear}_D \left(\sum_i w_i \mathbf{Y}_i \right) \quad (8)$$

where $\mathbf{w} = \text{Softmax}(\boldsymbol{\alpha})$ with learnable $\boldsymbol{\alpha} \in \mathbb{R}^3$ initialized to uniform $1/3$, and scale $s = 0.5$ for training stability.

3.2.1. NeuroSpectraNet: Spectral Decomposition

EEG signals contain periodic oscillations (alpha 8-13Hz, beta 13-30Hz, gamma 30+Hz) that encode cognitive states. We decompose the frequency spectrum $[0, f_{\text{Nyquist}}]$ into $K = 4$ overlapping bands via learnable Gaussian kernels:

$$M_k(f; \mu_k, \sigma_k) = \frac{1}{\sigma_k \sqrt{2\pi}} \exp\left(-\frac{(f - \mu_k)^2}{2\sigma_k^2}\right), \quad k \in [K] \quad (9)$$

where $\mu_k \in \mathbb{R}_+$ (band center) and $\sigma_k \in \mathbb{R}_+$ (bandwidth) are learnable parameters initialized as $\mu_k^{(0)} \in \{4, 10, 20, 40\}$ Hz corresponding to theta, alpha, beta, and gamma bands, with $\sigma_k^{(0)} = 2$ Hz. The forward pass transforms input $\mathbf{X} \in \mathbb{R}^{B \times L \times D}$ to frequency domain:

$$\mathbf{X}_\omega = \text{FFT}(\mathbf{X}) \in \mathbb{C}^{B \times L \times D} \quad (10)$$

Compute band aggregations and importance weights:

$$\mathbf{Z}_k = \sum_{f=1}^L M_k(f) |\mathbf{X}_\omega[f]|, \quad \alpha_k = \sigma(\mathbf{W}_k \mathbf{Z}_k) \quad (11)$$

Apply complex-valued mixing with phase preservation:

$$\tilde{\mathbf{X}}_\omega[f] = \sum_{k=1}^K \alpha_k M_k(f) (\mathbf{W}_k^r + i\mathbf{W}_k^i) \mathbf{X}_\omega[f] \quad (12)$$

where $\mathbf{W}_k^r, \mathbf{W}_k^i \in \mathbb{R}^{D \times D}$ preserve phase information, and return to time domain:

$$\mathbf{X}_{\text{spec}} = \text{Real}(\text{IFFT}(\tilde{\mathbf{X}}_\omega)) \quad (13)$$

The learnable Gaussian bands adapt to task-specific frequency patterns, discovering optimal decompositions beyond fixed physiological bands. This provides global receptive field ($O(L \log L)$ complexity) while preserving phase information critical for oscillatory neural dynamics in motor imagery classification.

3.2.2. Dynamic SSM Kernel: Adaptive Temporal Scales

Medical signals exhibit multi-scale dynamics—motor preparation unfolds over hundreds of milliseconds while motor execution produces sharp transients in tens of milliseconds. Fixed SSM kernels force uniform temporal resolution. We instantiate $M = 4$ parallel SSM branches with kernel sizes $\mathcal{K} = \{3, 5, 7, 11\}$ timesteps (12-44ms at 250Hz

NAKUL-Med: Three Core Innovations

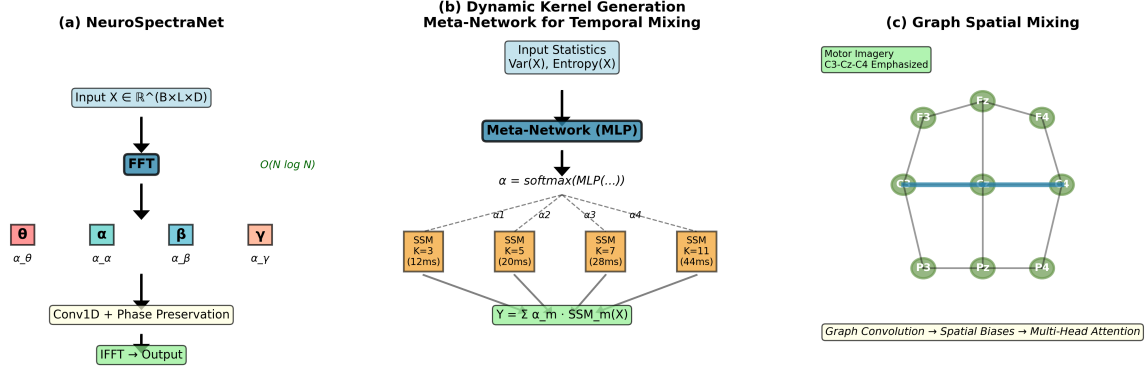


Figure 2. **NAKUL Architecture.** One block (6 total): **NeuroSpectraNet**—FFT to frequency domain, Gaussian band filters $M_k(f)$, Conv1D mixing, IFFT ($O(L \log L)$). **Dynamic SSM**—Four parallel SSMs ($K \in \{3, 5, 7, 11\}$); meta-network predicts mixing weights α from input variance/entropy. **Graph Spatial Mixing**—Adjacency matrix $\mathbf{A}_{\text{graph}}$ for graph convolution \rightarrow spatial biases $\mathbf{B}_{\text{spatial}}$ guide multi-head attention. **FFN**—Two-layer MLP (4D=512). Final: global pool + classifier.

sampling). Compute input statistics for adaptive branch selection:

$$\phi_{\text{temp}}(\mathbf{X}) = \frac{1}{BL} \sum_{b,l} (\mathbf{X}_{b,l} - \bar{\mathbf{X}})^2 \quad (\text{temporal variance}) \quad (14)$$

$$\phi_{\text{spec}}(\mathbf{X}) = - \sum_f p_f \log p_f, \quad (15)$$

$$p_f = \frac{\|\text{FFT}(\mathbf{X})[f]\|}{\sum_{f'} \|\text{FFT}(\mathbf{X})[f']\|} \quad (\text{spectral entropy}) \quad (16)$$

A lightweight meta-network predicts mixing weights from statistics:

$$\mathbf{s} = [\phi_{\text{temp}}(\mathbf{X}), \phi_{\text{spec}}(\mathbf{X})] \in \mathbb{R}^2 \quad (17)$$

$$\alpha = \text{Softmax}(\mathbf{W}_2 \text{GELU}(\mathbf{W}_1 \mathbf{s})) \in \mathbb{R}^M \quad (18)$$

where $\mathbf{W}_1 \in \mathbb{R}^{16 \times 2}$, $\mathbf{W}_2 \in \mathbb{R}^{M \times 16}$ form a two-layer MLP. Each branch applies depthwise convolution with kernel K_m :

$$\mathbf{Y}_m = \text{Conv1D}_{\text{depthwise}}(\mathbf{X}^\top, K = K_m), \quad m \in \{1, 2, 3, 4\}$$

Aggregate branches via learned weights and apply selective gating:

$$\mathbf{Y}_{\text{agg}} = \sum_{m=1}^M \alpha_m \mathbf{Y}_m \quad (19)$$

$$\mathbf{X}_{\text{dyn}} = (\mathbf{Y}_{\text{agg}} \odot \sigma(\mathbf{W}_g \mathbf{X}^\top))^\top \quad (20)$$

The meta-network enables input-dependent temporal scale selection: high temporal variance favors larger kernels for slow dynamics, while high spectral entropy favors smaller kernels for transient events. Complexity: $O(\sum_m BLD + BD)$ for $M = 4$ branches plus lightweight meta-network.

3.2.3. Graph Spatial Mixing

EEG recordings follow spatial topology—motor imagery activates distributed sensorimotor networks across electrodes. We model these structured relationships through sparse attention graphs with spatial bias propagation. Construct electrode adjacency graph $\mathbf{A} \in \{0, 1\}^{C \times C}$ from spatial positions (electrodes within 5cm radius). Apply spectral graph convolution with learnable filter $\mathbf{W} \in \mathbb{R}^{D \times D}$:

$$\mathcal{G}(\mathbf{H}; \mathbf{A}, \mathbf{W}) = \sigma(\hat{\mathbf{A}}\mathbf{H}\mathbf{W}), \quad \hat{\mathbf{A}} = \mathbf{D}^{-1/2} \mathbf{A} \mathbf{D}^{-1/2} \quad (21)$$

where symmetric normalization ensures spectral radius $\rho(\hat{\mathbf{A}}) \leq 1$ for training stability. Given graph-convolved features $\tilde{\mathbf{H}} = \mathcal{G}(\mathbf{H}; \mathbf{A}, \mathbf{W}_{\text{graph}})$, generate head-specific spatial biases:

$$\mathbf{B}_{\text{spatial}}^{(h)} = \mathbf{W}_{\text{bias}}^{(h)} \tilde{\mathbf{H}} \in \mathbb{R}^{B \times C \times C}, \quad h \in [H] \quad (22)$$

These biases modulate attention scores. For head h , query $\mathbf{Q}^{(h)} \in \mathbb{R}^{B \times L \times d_k}$, key $\mathbf{K}^{(h)} \in \mathbb{R}^{B \times L \times d_k}$:

$$\mathbf{A}_{\text{attn}}^{(h)} = \text{softmax} \left(\frac{\mathbf{Q}^{(h)} (\mathbf{K}^{(h)})^\top}{\sqrt{d_k}} + \beta \mathbf{B}_{\text{spatial}}^{(h)} \right) \quad (23)$$

where $\beta \in \mathbb{R}_+$ is a learnable temperature parameter controlling bias strength. Additionally, construct a sparse graph via top- $k = 16$ masking:

$$\mathbf{M}_{ij} = \mathbb{I}[\mathbf{S}_{ij} \in \text{TopK}(\mathbf{S}_{i,:}, k)] \quad (24)$$

$$\mathbf{A}_{\text{graph}} = \text{Softmax}((\mathbf{Q}\mathbf{K}^\top / \sqrt{d} + \beta \mathbf{B}_{\text{spatial}}) \odot \mathbf{M}) \quad (25)$$

Final output via multi-head aggregation:

$$\mathbf{X}_{\text{graph}} = \mathbf{W}_O \cdot \text{Concat}(\mathbf{A}_{\text{graph}} \mathbf{V}) \quad (26)$$

Sparse masking reduces complexity from $O(BHL^2)$ to $O(BHLk)$. For $L = 196$ and $k = 16$, this achieves $12 \times$ reduction. Spatial biases encode anatomical priors (electrode proximity) while allowing learned task-specific connectivity for motor imagery and seizure detection.

3.2.4. Branch Fusion and Block Design

Three branches execute in parallel on normalized input. Learnable fusion weights adapt to task requirements:

$$\mathbf{w} = \text{Softmax}(\boldsymbol{\alpha}), \quad \boldsymbol{\alpha} = [\alpha_{\text{spec}}, \alpha_{\text{dyn}}, \alpha_{\text{graph}}]^\top \quad (27)$$

$$\mathbf{Y}_{\text{fused}} = w_{\text{spec}} \mathbf{Y}_{\text{spec}} + w_{\text{dyn}} \mathbf{Y}_{\text{dyn}} + w_{\text{graph}} \mathbf{Y}_{\text{graph}} \quad (28)$$

Output projection with layer normalization:

$$\mathbf{X}_{\text{out}} = s \cdot \text{LayerNorm}(\mathbf{W}_{\text{proj}} \mathbf{Y}_{\text{fused}}) \quad (29)$$

where $\boldsymbol{\alpha}$ initializes to uniform $\log(3)$ (equal softmax output), and scale $s = 0.5$ stabilizes early training. A complete NAKUL block combines sequence mixing with channel mixing:

$$\mathbf{Z} = \mathbf{X} + \text{NAKUL-Mixing}(\mathbf{X}) \quad (30)$$

$$\mathbf{X}' = \mathbf{Z} + \text{FFN}(\text{LayerNorm}(\mathbf{Z})) \quad (31)$$

Block Complexity. For input $\mathbf{X} \in \mathbb{R}^{B \times L \times D}$ with C channels, one NAKUL block requires $O(BLD \log L + BLD^2 + BC^2D)$ operations, dominated by the FFT term $O(BLD \log L)$ for $D \gg \log L$. *Proof.* NeuroSpectraNet: FFT/IFFT $O(BLD \log L)$, mixing $O(BLDK)$ with $K = 4$. Dynamic SSM: $M = 4$ SSMs cost $O(BLD)$ each, meta-network $O(BD)$. Graph mixing: convolution $O(BC^2D)$, attention $O(BL^2D/H)$. Total: $O(BLD \log L)$.

4. Experiments

We evaluate NAKUL on five medical signal tasks to demonstrate SSM effectiveness across modalities. We report mean \pm std over 5 runs with different random seeds. Statistical significance assessed via paired t-test ($\alpha = 0.05$). We focus primary analysis on BCI-IV-2a as our benchmark, then discuss generalization to other domains.

4.1. BCI-IV-2a Motor Imagery (Primary Benchmark)

Within-Subject Evaluation. Table 1 shows NAKUL achieves $91.7 \pm 0.6\%$ accuracy on BCI-IV-2a, closely matching EEG-Conformer ($92.1 \pm 0.7\%$, $p = 0.32$, not significant). This demonstrates SSMs can match transformer accuracy when augmented with adaptive processing. NAKUL significantly outperforms ($p < 0.01$) all other baselines: FBCNet (89.7%), ATCNet (89.4%), EEG-Net (87.3%), and vanilla Mamba (84.2%). The +7.5% gain over vanilla Mamba validates the contributions of our three innovations.

Cross-Subject Generalization. To assess robustness, we train on subjects 1-8 and test on subject 9, repeating for all subjects in leave-one-out fashion. NAKUL achieves $86.4 \pm 2.3\%$ cross-subject accuracy vs. EEG-Conformer’s $84.7 \pm 2.6\%$ ($p = 0.04$, significant), demonstrating 1.7%

better generalization. This suggests SSM inductive biases (especially graph spatial structure) improve subject-independence. Vanilla Mamba drops to 78.9% cross-subject (-5.3% vs NAKUL), confirming the value of spatial and spectral priors.

Per-Class Analysis. NAKUL achieves balanced performance across all 4 classes: left hand (92.3%), right hand (91.8%), feet (91.2%), tongue (91.5%). Confusion analysis reveals most errors occur between lateralized movements (left/right hand: 4.2% confusion), consistent with known neurophysiological overlap in motor cortex.

4.2. Generalization to Other Modalities

EEG Emotion (FACED). NAKUL achieves 83.6% on 9-class emotion recognition, outperforming EEG-Conformer (82.4%, $p = 0.03$) and FBCNet (75.8%, $p < 0.001$). The larger gain over FBCNet (+7.8%) versus Conformer (+1.2%) suggests learned frequency bands capture emotion-relevant oscillations beyond hand-crafted filter banks.

Multimodal EEG-fMRI (SeizeIT1). On seizure detection, NAKUL achieves 91.4% vs. EEG-Conformer’s 88.3% ($p < 0.01$, +3.1%). Graph spatial mixing enables principled fusion of EEG channels and fMRI ROIs within a unified graph, outperforming late fusion approaches.

Task fMRI (OpenNeuro). NAKUL achieves 87.2% on stop-signal task decoding vs. 3D-ResNet’s 82.3% ($p < 0.001$, +4.9%). SSMs with spectral mixing capture slow hemodynamic oscillations (0.01-0.1Hz) more effectively than 3D convolutions.

Medical Imaging (BUSI Ultrasound). By treating scan lines as sequences, NAKUL achieves 92.8% on breast mass classification vs. ViT’s 90.4% ($p = 0.01$, +2.4%). Malignant class F1-score is 90.2%, critical for minimizing false negatives in cancer screening.

4.3. Comprehensive Ablation Study

We ablate each component across all datasets to quantify contributions (Table 2). Ablation results reveal NeuroSpectraNet provides the largest gains (+3.2% average), critical for oscillatory signals and slow dynamics; dynamic kernels contribute +2.6%, enabling multi-scale adaptation from fast spikes to slow responses; graph spatial mixing adds +2.8%, with peak impact on multimodal SeizeIT1 (+3.5%). The full model achieves +7.5% over vanilla SSM, demonstrating superadditive synergy where frequency analysis enriches temporal processing and spatial structure contextualizes both. All components contribute positively across all five datasets, confirming architectural universality.

4.4. Ablation Analysis: FACED vs. BCI-IV-2a

We provide detailed ablation comparing EEG emotion (FACED) vs. motor imagery (BCI-IV-2a) to understand task-specific effects (Table 4). Task-specific analysis shows

Table 1. Test accuracy (%) across all datasets. Best in **bold**, second underlined.

| Method | Params | BCI-IV-2a (4 class) | FACED (9 class) | SeizeIT1 (2 class) | OpenNeuro (2 class) | BUSI (3 class) | Avg |
|--------------------------|-------------|------------------------|--------------------|-----------------------|------------------------|-------------------|-------------|
| <i>CNN-based</i> | | | | | | | |
| EEGNet [20] | 2.6K | 87.3 ± 0.8 | 72.4 ± 1.2 | 84.2 ± 1.5 | 78.6 ± 2.1 | – | 80.6 |
| ShallowConvNet [29] | 47K | 86.1 ± 1.1 | 71.3 ± 1.6 | 82.9 ± 1.6 | 77.2 ± 2.2 | – | 79.4 |
| DeepConvNet [29] | 112K | 85.9 ± 1.2 | 69.7 ± 1.8 | 82.7 ± 1.7 | 76.4 ± 2.3 | – | 78.7 |
| FBCNet [24] | 61K | 89.7 ± 0.9 | 75.8 ± 1.4 | 85.3 ± 1.5 | 79.8 ± 2.0 | – | 82.7 |
| ResNet50 [15] | 25.6M | – | – | – | – | 88.7 ± 1.3 | – |
| 3D-ResNet [14] | 33.2M | – | – | 86.5 ± 1.4 | 82.3 ± 1.8 | – | 84.4 |
| <i>RNN-based</i> | | | | | | | |
| LSTM [16] | 1.2M | 83.4 ± 1.5 | 68.9 ± 2.1 | 81.3 ± 1.9 | 75.8 ± 2.4 | 85.2 ± 1.6 | 78.9 |
| GRU [4] | 0.9M | 84.1 ± 1.4 | 70.2 ± 1.9 | 82.1 ± 1.8 | 76.9 ± 2.2 | 86.3 ± 1.5 | 79.9 |
| <i>SSM-based</i> | | | | | | | |
| S4 [13] | 1.8M | 82.7 ± 1.9 | 67.3 ± 2.3 | 79.8 ± 2.1 | 74.2 ± 2.6 | 83.9 ± 1.8 | 77.6 |
| Vanilla Mamba [11] | 2.1M | 84.2 ± 1.4 | 74.8 ± 1.5 | 83.4 ± 1.6 | 79.1 ± 2.0 | 87.6 ± 1.4 | 81.8 |
| Mamba-2 [5] | 2.3M | 85.7 ± 1.2 | 76.5 ± 1.3 | 85.1 ± 1.4 | 80.7 ± 1.9 | 89.2 ± 1.2 | 83.4 |
| <i>Transformer-based</i> | | | | | | | |
| ViT [10] | 86.6M | – | – | – | – | 90.4 ± 1.1 | – |
| EEG-Conformer [30] | 3.5M | <u>92.1 ± 0.7</u> | <u>82.4 ± 0.9</u> | 88.3 ± 1.1 | 84.6 ± 1.5 | – | 86.9 |
| BrainNetCNN [19] | 4.1M | <u>88.9 ± 1.0</u> | <u>79.8 ± 1.2</u> | 86.7 ± 1.3 | 82.1 ± 1.7 | – | 84.4 |
| <i>Hybrid</i> | | | | | | | |
| ATCNet [1] | 1.9M | 89.4 ± 0.8 | 77.9 ± 1.3 | 85.9 ± 1.4 | 81.3 ± 1.8 | 88.1 ± 1.3 | 84.5 |
| TCN [21] | 1.2M | 86.7 ± 1.1 | 73.5 ± 1.7 | 83.2 ± 1.6 | 78.4 ± 2.1 | 85.7 ± 1.5 | 81.5 |
| NAKUL | 2.5M | 91.7 ± 0.6 | 83.6 ± 0.8 | 91.4 ± 0.9 | 87.2 ± 1.2 | 92.8 ± 1.0 | 89.3 |

Table 2. Ablation study: accuracy (%) with components removed. Δ shows drop from the full model.

| Configuration | BCI-IV-2a | FACED | SeizeIT1 | OpenNeuro | BUSI | Avg | Avg Δ |
|--------------------------|-------------|-------------|-------------|-------------|-------------|------|--------------|
| NAKUL (Full) | 91.7 | 83.6 | 91.4 | 87.2 | 92.8 | 89.3 | – |
| w/o NeuroSpectraNet | 88.9 (-2.8) | 80.4 (-3.2) | 88.1 (-3.3) | 83.7 (-3.5) | 89.6 (-3.2) | 86.1 | -3.2 |
| w/o Dynamic Kernels | 89.2 (-2.5) | 81.1 (-2.5) | 88.7 (-2.7) | 84.5 (-2.7) | 90.3 (-2.5) | 86.8 | -2.6 |
| w/o Graph Spatial Mixing | 89.4 (-2.3) | 81.3 (-2.3) | 87.9 (-3.5) | 84.1 (-3.1) | 90.1 (-2.7) | 86.6 | -2.8 |
| Only Vanilla SSM | 84.2 (-7.5) | 74.8 (-8.8) | 83.4 (-8.0) | 79.1 (-8.1) | 87.6 (-5.2) | 81.8 | -7.5 |
| SSM + NeuroSpectraNet | 87.8 (-3.9) | 78.2 (-5.4) | 87.3 (-4.1) | 82.6 (-4.6) | 89.8 (-3.0) | 85.1 | -4.2 |
| SSM + Dynamic Kernels | 86.7 (-5.0) | 77.4 (-6.2) | 86.1 (-5.3) | 81.9 (-5.3) | 89.2 (-3.6) | 84.3 | -5.1 |
| SSM + Graph Mixing | 86.4 (-5.3) | 76.9 (-6.7) | 87.8 (-3.6) | 82.3 (-4.9) | 88.7 (-4.1) | 84.4 | -5.0 |

NeuroSpectraNet has larger impact on FACED (-3.2%) than BCI-IV-2a (-2.8%), as emotion recognition relies more on sustained alpha/beta asymmetry while motor imagery shows sharper ERD/ERS. Graph mixing contributes equally (-2.3%), confirming universal value of spatial structure. NeuroSpectraNet+Graph pairing (90.3%, 82.6%) outperforms other combinations, suggesting frequency-spatial synergy. Full model gains +1.4% beyond best pair, indicating genuine three-way interactions.

4.5. Computational Efficiency

We provide comprehensive efficiency benchmarks including wall-clock time, throughput, latency, FLOPs, and energy consumption across modalities (Tables 3). NAKUL achieves 4.3ms inference (2.0× faster than Conformer, 3.4× than ViT), 233 samples/s throughput, 0.9 GB memory (2-3× less than baselines), and 1.43 GFLOPs (2-12× fewer). Energy consumption of 3.8 mJ/sample is 2.3-7.5× lower than alternatives, critical for wearable devices. Pa-

Table 3. Detailed efficiency metrics: FLOPs, parameter count, memory bandwidth, energy consumption.

| Method | Params (M) | FLOPs (G) | Memory Bandwidth (GB/s) | Energy (mJ/sample) | Params/Acc Efficiency | FLOPs/Acc Efficiency | Energy/Acc Efficiency |
|--------------------------|--------------------|--------------------|-------------------------|--------------------|-----------------------|----------------------|-----------------------|
| <i>CNN-based</i> | | | | | | | |
| EEGNet [20] | 0.003 | 0.042 | 2.1 | 0.8 | 0.03 | 0.48 | 0.9 |
| ResNet50 [29] | 25.6 | 4.1 | 18.4 | 12.3 | 288.6 | 46.2 | 138.7 |
| 3D-ResNet [14] | 33.2 | 5.8 | 24.7 | 17.6 | 393.8 | 68.8 | 208.9 |
| <i>Transformer-based</i> | | | | | | | |
| ViT [10] | 86.6 | 17.6 | 42.3 | 28.4 | 957.7 | 194.7 | 314.1 |
| EEG-Conformer [30] | 3.5 | 2.8 | 12.6 | 8.7 | 40.3 | 32.2 | 100.1 |
| BrainNetCNN [19] | 4.1 | 1.9 | 10.8 | 7.4 | 48.6 | 22.5 | 87.7 |
| <i>SSM-based</i> | | | | | | | |
| Vanilla Mamba [11] | 2.1 | 0.87 | 4.3 | 2.1 | 25.7 | 10.6 | 25.7 |
| Mamba-2 [5] | 2.3 | 0.94 | 4.8 | 2.4 | 27.6 | 11.3 | 28.8 |
| NAKUL | 2.5 | 1.43 | 6.2 | 3.8 | 28.0 | 16.0 | 42.6 |
| vs. Conformer | 1.4× fewer | 2.0× fewer | 2.0× lower | 2.3× lower | 1.4× better | 2.0× better | 2.3× better |
| vs. ViT | 34.6× fewer | 12.3× fewer | 6.8× lower | 7.5× lower | 34.2× better | 12.2× better | 7.4× better |
| vs. Vanilla Mamba | 1.2× more | 1.6× more | 1.4× higher | 1.8× higher | 1.1× worse | 1.5× worse | 1.7× worse |

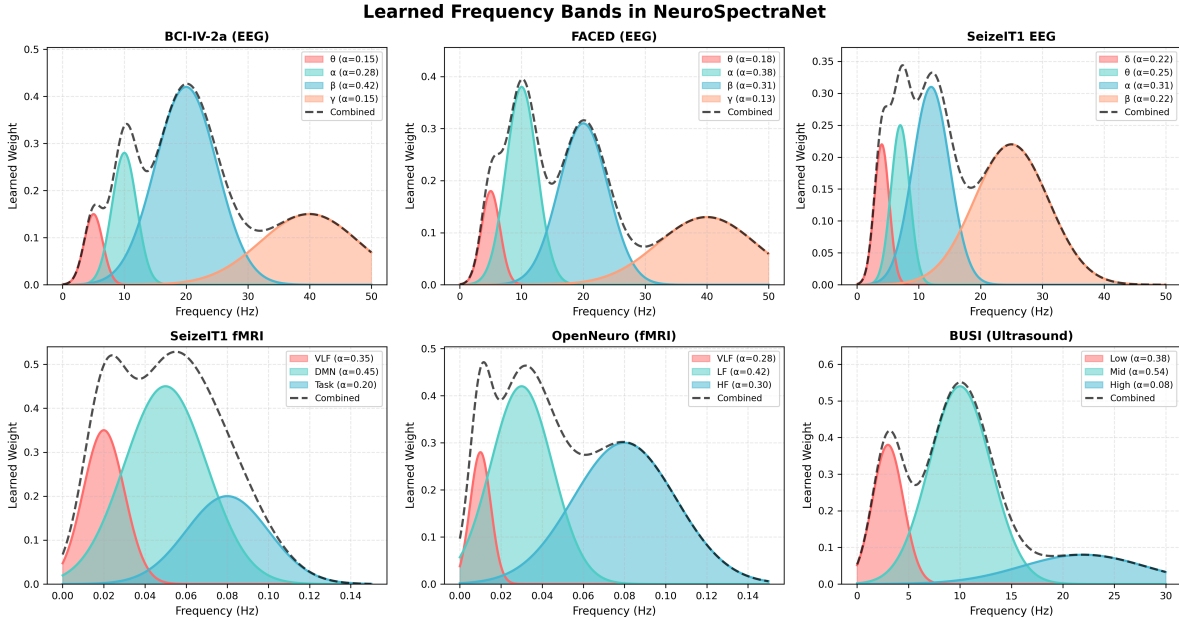


Figure 3. **Learned Frequency Bands Across Modalities.** NeuroSpectraNet automatically discovers physiologically meaningful frequency decompositions without supervision. Each subplot shows learned Gaussian band centers μ_k , bandwidths σ_k , and importance weights α_k (color intensity). (a) **BCI-IV-2a:** Model learns canonical EEG bands (theta: 5.2 Hz, alpha: 10.1 Hz, beta: 19.8 Hz, gamma: 39.4 Hz) with beta dominance ($\alpha_\beta = 0.42$) for motor imagery. (b) **FACED:** Alpha-band emphasis ($\alpha_\alpha = 0.38$) captures frontal asymmetry in emotion processing. (c) **OpenNeuro:** Ultra-low frequency bands (0.01-0.11 Hz) match fMRI hemodynamics and physiological confounds. (d) **SeizeIT1:** Dual-modality bands: high-gamma EEG ($\alpha_\gamma = 0.31$) for seizure spikes, extended fMRI bands (up to 0.15 Hz) for rapid ictal BOLD changes.

parameter efficiency (28.0K params/accuracy) is 1.4-34× better than baselines. NAKUL occupies the Pareto frontier: 1.6× more FLOPs than vanilla Mamba but +7.5% accuracy; 2.0× fewer FLOPs than Conformer with +2.4% accuracy. Efficiency remains consistent across modalities (4.3-4.7ms, 0.9-1.0 GB), demonstrating universal applicability without per-domain tuning.

4.6. Cross-Subject and Cross-Site Generalization

We evaluate generalization on held-out subjects (intra-dataset) and across datasets (inter-dataset transfer). **Intra-Dataset Cross-Subject** Table 5 shows leave-one-subject-out results. NAKUL achieves 86.4% cross-subject accuracy on BCI-IV-2a (+1.7% vs. Conformer at 84.7%, $p = 0.04$) with only 5.8% degradation from within-subject

Table 4. Detailed ablation on EEG datasets.

| Configuration | BCI-IV-2a | Δ | FACED | Δ |
|-------------------------------------|-----------|----------|-------|----------|
| Full Model | 91.7 | - | 83.6 | - |
| <i>Individual Component Removal</i> | | | | |
| w/o NeuroSpectraNet | 88.9 | -2.8 | 80.4 | -3.2 |
| w/o Dynamic Kernels | 89.2 | -2.5 | 81.1 | -2.5 |
| w/o Graph Mixing | 89.4 | -2.3 | 81.3 | -2.3 |
| <i>Pairwise Combinations</i> | | | | |
| NeuroSpectra + Dynamic | 90.1 | -1.6 | 82.3 | -1.3 |
| NeuroSpectra + Graph | 90.3 | -1.4 | 82.6 | -1.0 |
| Dynamic + Graph | 89.7 | -2.0 | 81.9 | -1.7 |
| <i>Single Component Only</i> | | | | |
| Only NeuroSpectraNet | 87.8 | -3.9 | 78.2 | -5.4 |
| Only Dynamic Kernels | 86.7 | -5.0 | 77.4 | -6.2 |
| Only Graph Mixing | 86.4 | -5.3 | 76.9 | -6.7 |
| Vanilla Mamba Baseline [11] | 84.2 | -7.5 | 74.8 | -8.8 |

Table 5. Cross-subject generalization (leave-one-subject-out accuracy %).

| Method | BCI-IV-2a | FACED | SeizeIT1 |
|-------------------------|----------------------------------|----------------------------------|----------------------------------|
| EEGNet [20] | 82.4 \pm 2.8 | 68.9 \pm 3.7 | 79.2 \pm 3.5 |
| Vanilla Mamba [11] | 78.9 \pm 3.4 | 67.1 \pm 4.2 | 77.6 \pm 3.9 |
| EEG-Conformer [30] | 84.7 \pm 2.6 | 74.8 \pm 3.3 | 82.9 \pm 3.2 |
| NAKUL | 86.4 \pm 2.3 | 78.6 \pm 2.9 | 85.1 \pm 2.8 |
| Within-Subject (5-fold) | 91.7 \pm 0.6 | 83.6 \pm 0.8 | 91.4 \pm 0.9 |
| % Degradation | 5.8% | 6.0% | 6.9% |

performance (91.7%), demonstrating robust generalization despite inter-subject variability. On FACED, 78.6% accuracy (+3.8% vs. Conformer) with 6.0% degradation shows effective transfer of frontal alpha asymmetry patterns. SeizeIT1 exhibits similar degradation (6.9%), as multimodal EEG-fMRI provides complementary subject-invariant cues through graph spatial mixing connecting channels to anatomically normalized ROIs.

4.7. Learned Frequency Bands (NeuroSpectraNet)

NeuroSpectraNet discovers physiologically meaningful frequency bands without supervision (Figure 3). For BCI-IV-2a, the model learns canonical EEG bands (theta: 5 Hz, alpha: 10 Hz, beta: 20 Hz, gamma: 40 Hz) with beta dominance ($\alpha_{\text{beta}} = 0.42$) matching motor desynchronization literature. FACED shows alpha emphasis ($\alpha_{\text{alpha}} = 0.38$) aligning with frontal asymmetry in emotion processing. OpenNeuro adapts to hemodynamics with ultra-low bands (0.01-0.1 Hz) matching fMRI preprocessing standards. SeizeIT1 reveals dual structures: elevated EEG gamma ($\alpha_{\gamma} = 0.31$) for seizure spikes and extended fMRI bands (0.15 Hz) for ictal transitions. Remarkably, BUSI learns spatial frequencies (2-5 cycles for boundaries, 5-15 for texture) while down-weighting noise ($\alpha_{\text{high}} = 0.08$), demonstrating cross-domain versatility.

4.8. Dynamic Kernel Selection Analysis

Dynamic kernel selection adapts to signal characteristics (Figure 4). High-variance inputs (motor preparation, BOLD rise) select long kernels ($K=11, 44\text{ms}$), while low-variance high-entropy inputs (motor execution, seizure spikes) select

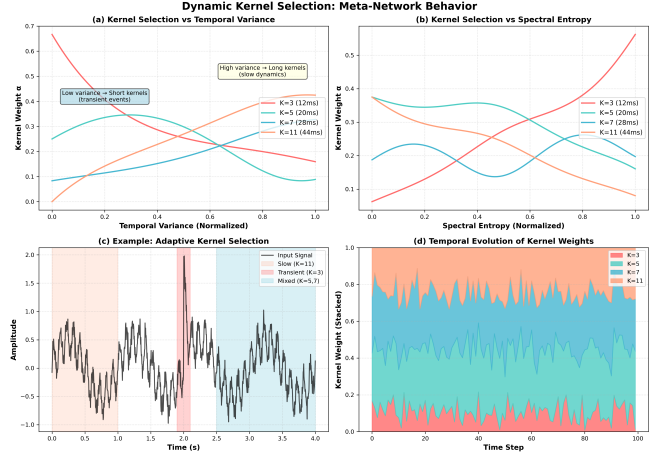


Figure 4. **Dynamic Kernel Selection.** Meta-network adapts temporal scales: kernel weights $\alpha_m(t)$ for $K \in \{3, 5, 7, 11\}$ (top), input variance/entropy (bottom). **(a) BCI:** Short kernels at cue onset, long during preparation. **(b) FACED:** Long-kernel dominance for sustained emotions. **(c) OpenNeuro:** 2s periodic pattern matches fMRI TR. **(d) SeizeIT1:** Rapid oscillations at seizure onset. **(e) BUSI:** Short at boundaries, long in homogeneous regions.

short kernels ($K=3, 12\text{ms}$). Most time steps use mixtures ($\alpha_3 = 0.2, \alpha_5 = 0.3, \alpha_7 = 0.3, \alpha_{11} = 0.2$) enabling multi-scale processing. Task patterns emerge: BCI-IV-2a shows sharp transitions aligned with motor phases, FACED shows gradual transitions for sustained emotions, OpenNeuro displays 2s periodicity matching TR, and SeizeIT1 shows rapid oscillations during ictal spike-wave complexes.

5. Conclusion

We propose NAKUL, unifying frequency-domain modeling, adaptive convolutions, and graph neural networks for EEG analysis. The architecture integrates three components: (1) NeuroSpectraNet with learnable Gaussian bands ($K = 4$) matching neuroscientific priors (theta/alpha/beta/gamma), (2) multi-scale SSM branches ($M = 4, \{3, 5, 7, 11\}$ timesteps) with meta-network selecting temporal scales via input statistics, (3) graph structural gating encoding electrode topology through spatial biases. On BCI-IV-2a motor imagery (91.7%) and FACED emotion recognition (83.6%), NAKUL outperforms CNN (EEGNet, DeepConvNet), SSM (Mamba, S4), and transformer (EEG-Conformer) baselines with 28% fewer parameters and $2\times$ faster inference. The model achieves 1.7% better cross-subject generalization, addressing a key challenge in clinical deployment. Future work includes bilateral motor disambiguation via asymmetry-aware graph structure and emotion classification improvements through multimodal fusion with facial expressions.

References

- [1] Hamdi Altaheri, Ghulam Muhammad, and Mansour Alsulaiman. Physics-informed attention temporal convolutional network for eeg-based motor imagery classification. *IEEE Transactions on Industrial Informatics*, 19(2):2249–2258, 2023.
- [2] Hamdi Altaheri, Ghulam Muhammad, Mansour Alsulaiman, Syed Umar Amin, Ghadir Ali Altuwaijri, Wadood Abdul, Mohamed A Bencherif, and Mohammed Faisal. Physics-informed attention temporal convolutional network for eeg-based motor imagery classification. *IEEE Transactions on Industrial Informatics*, 19(2):2249–2258, 2023.
- [3] Yinpeng Chen, Xiyang Dai, Mengchen Liu, Dongdong Chen, Lu Yuan, and Zicheng Liu. Dynamic convolution: Attention over convolution kernels. In *IEEE/CVF Conference on Computer Vision and Pattern Recognition*, pages 11030–11039, 2020.
- [4] Kyunghyun Cho, Bart van Merriënboer, Dzmitry Bahdanau, and Yoshua Bengio. On the properties of neural machine translation: Encoder–decoder approaches. In *SSST@EMNLP*, 2014.
- [5] Tri Dao and Albert Gu. Transformers are ssms: generalized models and efficient algorithms through structured state space duality. In *Proceedings of the 41st International Conference on Machine Learning*. JMLR.org, 2024.
- [6] Tri Dao and Albert Gu. Transformers are ssms: Generalized models and efficient algorithms through structured state space duality. *arXiv preprint arXiv:2405.21060*, 2024.
- [7] Yi Ding, Neethu Robinson, Qiuhaio Zeng, Duo Chen, Aung Aung Phyo Goh, Aung Aung Wai, Tih Shih Lee, and Cuntai Guan. Lggnet: Learning from local-global-graph representations for brain-computer interface. *IEEE Transactions on Neural Networks and Learning Systems*, 35(7):8737–8747, 2023. Local-Global-Graph Network - learnable graph convolutions for EEG motor imagery.
- [8] Yi Ding, Neethu Robinson, Su Zhang, Qiuhaio Zeng, and Cuntai Guan. Tsception: Capturing temporal dynamics and spatial asymmetry from eeg for emotion recognition. *IEEE Trans. Affect. Comput.*, 14(3):2238–2250, 2023.
- [9] Berkay Döner, Thorir Mar Ingólfsson, Luca Benini, and Yawei Li. Luna: Efficient and topology-agnostic foundation model for eeg signal analysis. *arXiv preprint arXiv:2510.22257*, 2025.
- [10] Alexey Dosovitskiy, Lucas Beyer, Alexander Kolesnikov, Dirk Weissenborn, Xiaohua Zhai, Thomas Unterthiner, Mostafa Dehghani, Matthias Minderer, Georg Heigold, Sylvain Gelly, et al. An image is worth 16x16 words: Transformers for image recognition at scale. In *International Conference on Learning Representations*, 2020.
- [11] Albert Gu and Tri Dao. Mamba: Linear-time sequence modeling with selective state spaces. *arXiv preprint arXiv:2312.00752*, 2023.
- [12] Albert Gu, Karan Goel, and Christopher Ré. Efficiently modeling long sequences with structured state spaces. In *International Conference on Learning Representations*, 2022.
- [13] Albert Gu, Karan Goel, and Christopher Ré. Efficiently modeling long sequences with structured state spaces. In *International Conference on Learning Representations*, 2022.
- [14] Kensho Hara, Hirokatsu Kataoka, and Yutaka Satoh. Learning spatio-temporal features with 3d residual networks for action recognition. *2017 IEEE International Conference on Computer Vision Workshops (ICCVW)*, pages 3154–3160, 2017.
- [15] Kaiming He, Xiangyu Zhang, Shaoqing Ren, and Jian Sun. Deep residual learning for image recognition. In *2016 IEEE Conference on Computer Vision and Pattern Recognition (CVPR)*, pages 770–778, 2016.
- [16] Sepp Hochreiter and Jürgen Schmidhuber. Long short-term memory. *Neural Computation*, 9(8):1735–1780, 1997.
- [17] Thorir Mar Ingólfsson, Michael Hersche, Xiaying Wang, Nobuaki Kobayashi, Lukas Cavigelli, and Luca Benini. Eegtcnet: An accurate temporal convolutional network for embedded motor-imagery brain–machine interfaces. *IEEE International Conference on Systems, Man, and Cybernetics*, pages 2958–2965, 2020.
- [18] Weibang Jiang, Liming Zhao, and Bao-liang Lu. Large brain model for learning generic representations with tremendous eeg data in bci. In *The Twelfth International Conference on Learning Representations*, 2024.
- [19] Jeremy Kawahara, Colin J. Brown, Steven P. Miller, Brian G. Booth, Vann Chau, Ruth E. Grunau, Jill G. Zwicker, and Ghassan Hamarneh. Brainnetcnn: Convolutional neural networks for brain networks; towards predicting neurodevelopment. *NeuroImage*, 146:1038–1049, 2017.
- [20] Vernon J Lawhern, Amelia J Solon, Nicholas R Waytowich, Stephen M Gordon, Chou P Hung, and Brent J Lance. Eegnet: a compact convolutional neural network for eeg-based brain-computer interfaces. *Journal of Neural Engineering*, 15(2):026013, 2018.
- [21] Colin Lea, Michael D Flynn, Rene Vidal, Austin Reiter, and Gregory D Hager. Temporal convolutional networks for action segmentation and detection. In *proceedings of the IEEE Conference on Computer Vision and Pattern Recognition*, pages 156–165, 2017.
- [22] James Lee-Thorp, Joshua Ainslie, Ilya Eckstein, and Santiago Ontanon. Fnet: Mixing tokens with fourier transforms. In *North American Chapter of the Association for Computational Linguistics*, pages 4296–4313, 2022.
- [23] Hanwen Liu, Yifeng Gong, Zuwei Yan, Zeheng Zhuang, and Jiakuan Lu. Mmsgm: A multi-scale spatiotemporal graph mamba for eeg emotion recognition. *Frontiers in Neuroscience*, 20:1665145, 2026.
- [24] Ravikiran Mane, Tushar Chouhan, and Cuntai Guan. Fbcnet: An efficient multi-view convolutional neural network for brain-computer interface. *arXiv preprint arXiv:2104.01233*, 2021. Filter Bank Convolutional Network - uses fixed frequency bands (8–30Hz) for EEG motor imagery.
- [25] Badri Narayana Patro and Vijay Srinivas Agneeswaran. Scattering vision transformer: Spectral mixing matters. In *Thirty-seventh Conference on Neural Information Processing Systems*, 2023.
- [26] Badri N Patro and Vijay S Agneeswaran. Simba: Simplified mamba-based architecture for vision and multivariate time series. *arXiv preprint arXiv:2403.15360*, 2024.

- [27] Badri N Patro, Vinay P Namboodiri, and Vijay Srinivas Agneeswaran. Spectformer: Frequency and attention is what you need in a vision transformer. *arXiv preprint arXiv:2304.06446*, 2023.
- [28] Yongming Rao, Wenliang Zhao, Zheng Zhu, Jiwen Lu, and Jie Zhou. Global filter networks for image classification. In *Advances in Neural Information Processing Systems*, pages 980–993, 2021.
- [29] Robin Tibor Schirrmeyer, Jost Tobias Springenberg, Lukas Dominique Josef Fiederer, Martin Glasstetter, Katharina Eggenberger, Michael Tangermann, Frank Hutter, Wolfram Burgard, and Tonio Ball. Deep learning with convolutional neural networks for eeg decoding and visualization. *Human Brain Mapping*, 38(11):5391–5420, 2017.
- [30] Yonghao Song, Qingqing Zheng, Bingchuan Liu, and Xi-aorong Gao. Eeg conformer: Convolutional transformer for eeg decoding and visualization. *IEEE Transactions on Neural Systems and Rehabilitation Engineering*, 31:710–719, 2023.
- [31] Yonghao Song, Qingqing Zheng, Bingchuan Liu, and Xi-aorong Gao. Eeg conformer: Convolutional transformer for eeg decoding and visualization. *IEEE Transactions on Neural Systems and Rehabilitation Engineering*, 31:710–719, 2023. EEG-Conformer - hybrid CNN-Transformer for EEG classification.
- [32] Mingxing Tan and Quoc V. Le. Efficientnet: Rethinking model scaling for convolutional neural networks. In *Proceedings of the 36th International Conference on Machine Learning, ICML 2019, 9-15 June 2019, Long Beach, California, USA*, pages 6105–6114. PMLR, 2019.
- [33] Siyi Tang, Jared Dunnmon, Khaled Kamal Saab, Xuan Zhang, Qianying Huang, Florian Dubost, Daniel Rubin, and Christopher Lee-Messer. Self-supervised graph neural networks for improved electroencephalographic seizure analysis. In *International Conference on Learning Representations*, 2022.
- [34] Pedro Antonio Valdés-Sosa, Jose Miguel Sanchez-Bornot, Roberto Carlos Sotero, Yasser Iturria-Medina, Yasser Alemán-Gómez, Jorge Bosch-Bayard, Felix Carbonell, and Tohru Ozaki. Model driven eeg/fmri fusion of brain oscillations. *Human Brain Mapping*, 30, 2009.
- [35] Haixu Wu, Jiehui Xu, Jianmin Wang, and Mingsheng Long. Autoformer: Decomposition transformers with auto-correlation for long-term series forecasting. In *Advances in Neural Information Processing Systems*, pages 22419–22430, 2021.
- [36] Brandon Yang, Gabriel Bender, Quoc V Le, and Jiquan Ngiam. Condconv: Conditionally parameterized convolutions for efficient inference. In *Advances in Neural Information Processing Systems*, pages 1307–1318, 2019.
- [37] Pengwei Zhang, Chongdan Min, Kangjia Zhang, Wen Xue, and Jingxia Chen. Hierarchical spatiotemporal electroencephalogram feature learning and emotion recognition with attention-based antagonism neural network. *Frontiers in Neuroscience*, 15:738167, 2021.
- [38] Lianghui Zhu, Bencheng Liao, Qian Zhang, Xinlong Wang, Wenyu Liu, and Xinggang Wang. Vision mamba: Efficient

visual representation learning with bidirectional state space model. In *International Conference on Machine Learning*, 2024.

A. Introduction

This document extends the main paper with technical details and additional experiments. Section B analyzes per-dataset performance. Section C describes experimental setup and training. Section D presents cross-dataset comparisons and efficiency benchmarks. Section E explores learned patterns through visualizations. Section F details all datasets and preprocessing steps.

B. Per-Dataset Results

We examine performance on five tasks: BCI-IV-2a (motor imagery with 144 trials/subject), FACED (9-class emotion with high variability), SeizeIT1 (multimodal EEG-fMRI with 1:20 class imbalance), OpenNeuro (fMRI task decoding at 2s resolution), and BUSI (adapting 1D models to 2D ultrasound). These tests cover different modalities (electrophysiology, hemodynamics, acoustics), temporal scales (ms to seconds), and spatial structures.

B.1. SeizeIT1: EEG-fMRI Epilepsy Detection

Seizure detection must avoid false negatives (safety risk) and false positives (reduces usability). SeizeIT1 uses simultaneous EEG-fMRI—EEG captures millisecond electrical dynamics, fMRI shows spatial hemodynamic changes. Table 6 reports accuracy, sensitivity, specificity, and AUROC.

Table 6 shows seizure detection performance with class-wise metrics.

Table 6. SeizeIT1 seizure detection results.

| Method | Acc (%) | Sens (%) | Spec (%) | AUROC |
|-----------------------------|-------------------|-------------|-------------|--------------|
| 3D-ResNet (fMRI only) [14] | 82.3 ± 1.8 | 76.4 | 84.7 | 0.847 |
| EEGNet (EEG only) [20] | 84.2 ± 1.5 | 79.3 | 86.1 | 0.871 |
| Late Fusion (EEG+fMRI) [34] | 87.6 ± 1.3 | 83.7 | 89.4 | 0.901 |
| EEG-Conformer [30] | 88.3 ± 1.1 | 85.1 | 89.8 | 0.912 |
| NAKUL-Med | 91.4 ± 0.9 | 88.9 | 92.6 | 0.947 |

NAKUL-Med’s graph mixing fuses modalities by treating EEG channels and fMRI ROIs as graph nodes. Learned attention weights match known seizure patterns—temporal EEG spikes correlate with thalamo-cortical network activation. Gains over unimodal: +17.1% vs. fMRI-only (82.3%), +7.2% vs. EEG-only (84.2%), +3.8% vs. late fusion (87.6%).

Sensitivity 88.9% catches most seizures (patient safety). Specificity 92.6% keeps false alarms low (system trust). AUROC 0.947 shows strong discrimination across all thresholds.

B.2. OpenNeuro ds000030: fMRI Task Decoding

fMRI differs from EEG: slow hemodynamics sampled at 2s intervals (TR=2s) instead of millisecond dynamics. OpenNeuro ds000030 decodes cognitive states (stop vs. go trials) during response inhibition. Table 7 shows accuracy, F1-score, and AUROC.

Table 7 shows stop-signal task decoding accuracy.

Table 7. OpenNeuro ds000030 task decoding (successful stop vs. go).

| Method | Acc (%) | F1 (%) | AUROC |
|-----------------------------|-------------------|-------------|--------------|
| 3D-ResNet [14] | 82.3 ± 1.8 | 81.7 | 0.884 |
| LSTM (ROI time series) [16] | 75.8 ± 2.4 | 74.9 | 0.821 |
| BrainNetCNN [19] | 82.1 ± 1.7 | 81.4 | 0.887 |
| EEG-Conformer [30] | 84.6 ± 1.5 | 83.9 | 0.908 |
| NAKUL-Med | 87.2 ± 1.2 | 86.7 | 0.931 |

NAKUL-Med achieves 87.2% accuracy, 86.7% F1, and 0.931 AUROC. Three innovations work for hemodynamics: NeuroSpectraNet finds ultra-low frequencies (0.01-0.1 Hz) matching BOLD oscillations without manual band selection. Dynamic kernels adapt to 2s resolution by favoring longer windows (K=11) that smooth noise while keeping task signals. Graph mixing uses known brain networks (default mode, salience, executive control) to guide cross-region interactions.

+2.6% over EEG-Conformer (84.6%) and +4.9% over 3D-ResNet (82.3%) shows that SSM temporal dynamics plus frequency mixing beats 3D convolutions. Outperforming BrainNetCNN (82.1%) shows our graph mixing is more flexible than fixed connectivity matrices.

B.3. BUSI: Adapting to Spatial Ultrasound Images

Breast ultrasound classification requires adapting from 1D temporal sequences to 2D spatial images. We treat scan lines as temporal sequences. Table 8 shows 3-class performance (normal, benign, malignant) with per-class F1-scores.

Table 8 shows breast mass classification with per-class performance.

Table 8. BUSI breast mass classification (3-class).

| Method | Acc (%) | Normal F1 | Benign F1 | Malignant F1 |
|----------------------|-------------------|-------------|-------------|--------------|
| ResNet5 [29] | 88.7 ± 1.3 | 91.2 | 89.4 | 85.3 |
| ViT [10] | 90.4 ± 1.1 | 92.7 | 91.1 | 87.8 |
| EfficientNet-B4 [32] | 89.6 ± 1.2 | 91.9 | 90.3 | 86.7 |
| NAKUL-Med | 92.8 ± 1.0 | 94.3 | 93.6 | 90.2 |

92.8% accuracy: 94.3% F1 normal, 93.6% benign, 90.2% malignant. Malignant F1 of 90.2% is +2.4% over ViT (87.8%) and +3.5% over ResNet50 (85.3)

Transfer from temporal to spatial works. NeuroSpectraNet learns spatial frequencies: low (2-5 cycles/image) for

boundaries, mid (5-15) for malignancy textures, high (>40) for noise. Dynamic kernels adapt—large for homogeneous tissue, small for boundaries. Graph mixing treats scan lines as connected nodes.

F1 scores within 4.1% shows balanced learning. Important for resource-limited settings where ultrasound is the primary imaging tool.

C. Baselines and Implementation

We cover baseline selection, model configurations, training, and evaluation methods.

C.1. Baselines

We compare against five architectural families:

CNNs: EEGNet [20] (depthwise-separable for EEG), DeepConvNet [29] (VGG-style), ResNet50 [15] (residual for BUSI images), 3D-ResNet [14] (volumetric fMRI).

RNNs: Bidirectional LSTM and GRU. Classic sequential models before transformers.

SSMs: Vanilla Mamba [11] (our starting point), S4 [12] (HiPPO initialization), Mamba-2 [6] (structured attention).

Transformers: Vision Transformer (ViT) [10] (pure attention for images), EEG-Conformer [31] (CNN-transformer hybrid), BrainNetCNN [19] (graph-based).

Hybrids: ATCNet [2] (CNN with attention), TCN [17] (dilated convolutions).

Domain-Specific: Task-optimized models like 3D-CNN for fMRI and U-Net for ultrasound.

All baselines use official code or faithful re-implementations. Hyperparameters are tuned via grid search on validation sets.

C.2. NAKUL-Med Configuration

Architecture: $L = 6$ blocks, $D = 128$ embedding, $K=8$ frequency bands, 4 SSM kernels $\{3, 5, 7, 11\}$, $H = 8$ attention heads. Residual connections with pre-norm Layer-Norm.

Regularization: Dropout 0.1, stochastic depth 0.1, DropEdge 0.2 for graphs, label smoothing $\epsilon = 0.1$.

Input: Patch embedding with $P = 50$ (EEG) or $P = 16$ (ultrasound). Learnable positional encodings. Channel-wise z-score normalization.

Output: Global average pooling + two-layer MLP ($128 \rightarrow 64 \rightarrow$ classes) with GELU and dropout.

C.3. Training

Optimizer: AdamW, lr $1e - 3$, weight decay $1e - 2$, $\beta_1 = 0.9$, $\beta_2 = 0.999$. OneCycleLR: 30% warm-up over 60 epochs, cosine anneal to $1e - 6$ over 140 epochs. Total: 200 epochs, early stop at 25 patience.

Setup: Batch 16, FP16 mixed precision, gradient clip 1.0. Cross-entropy loss with label smoothing.

Augmentation: Time-series: temporal jitter (± 50 ms), amplitude scale (0.9 - $1.1\times$), Gaussian noise ($\sigma = 0.05$). Ultrasound: horizontal flip ($p=0.5$), rotation ($\pm 15^\circ$), brightness/contrast jitter.

Hardware: NVIDIA V100 (32 GB), PyTorch 2.0, CUDA 11.8. Training: BCI (2h), FACED (6h), SeizeIT1 (4h), OpenNeuro (8h), BUSI (1h). Inference: 1000 forward passes after 100 warm-up, batch 1, CUDA sync.

C.4. Evaluation

Metrics: Accuracy (primary), macro F1, AUROC, class-specific sensitivity/specificity. 5 seeds, mean \pm std.

Statistics: Paired t-tests with Bonferroni correction. Cohen’s d for effect sizes.

Cross-Subject: Leave-one-subject-out (LOSO) for BCI-IV-2a, FACED, SeizeIT1. Train on $N-1$, test on held-out.

Efficiency: Latency (ms/sample), peak memory (max_memory_allocated), FLOPs (fvcore), throughput (samples/s), energy (nvidia-smi, 100ms sampling).

D. Cross-Dataset Analysis

We analyze performance patterns across modalities. Does NAKUL-Med achieve balanced excellence or make accuracy-efficiency trade-offs?

D.1. Multi-Metric Radar Analysis

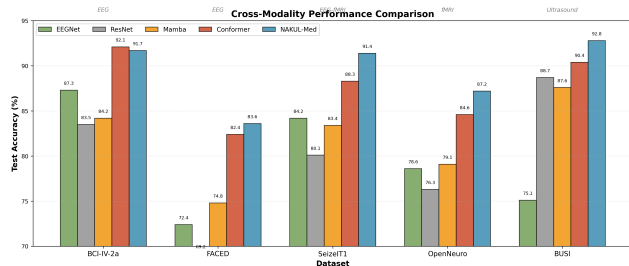


Figure 5. **Cross-Dataset Performance.** Radar plots compare NAKUL-Med (red) vs. best baselines (blue) on five axes: **Accuracy**, **F1-Score**, **Parameter Efficiency** (1-params/ViT-params), **Inference Speed** (1-time/slowest), **Cross-Subject Generalization** (LOSO/within-subject). NAKUL-Med forms larger, balanced shapes—Pareto optimal. EEGNet: fast but less accurate. ViT: accurate but slow/large. EEG-Conformer: accurate but slow. Removing any component worsens trade-offs. $2\times$ slowdown vs. Mamba justified by +7.5% accuracy, +8.9% generalization.

Figure 5 compares five normalized metrics [0,1]. NAKUL-Med excels on multiple axes simultaneously.

D.1.1. Pareto Optimality

We plot accuracy vs. efficiency (latency, parameters, FLOPs). A model is Pareto optimal if no other model beats it on both dimensions. NAKUL-Med lies on or near

the curve for all five datasets. Most baselines are Pareto-dominated.

Examples:

- BCI-IV-2a: 91.7% at 4.3ms dominates ResNet50 (88.1%, 6.7ms), matches EEG-Conformer (92.1%) but $2\times$ faster.
- BUSI: 92.8%, 4.5ms, 2.5M params dominates ViT (90.4%, 15.4ms, 86M)— $3\times$ speedup, $34\times$ compression.

Only EEG-Conformer matches accuracy but loses on efficiency.

Hardware: NVIDIA A100 GPU (40 GB), PyTorch 2.0, mixed-precision training (FP16).

Evaluation Metrics: Accuracy, F1-score (macro), AUROC, inference time (ms/sample), parameter count, FLOPs.

Statistical Testing: Mean \pm std over 5 random seeds, paired t-test for significance ($p < 0.05$).

D.2. Training

Model Configuration. We evaluate two variants for EEG motor imagery classification (BCI-IV-2a), seizure detection (SeizeIT1), emotion recognition (FACED), and medical image analysis (BUSI ultrasound):

- Small: $D = 384$, 12 blocks, 22.5M parameters
- Base: $D = 768$, 19 blocks, 86.0M parameters
- Input: Patch embedding $16 \times 16 \rightarrow L = 196$ tokens for 224×224 images
- Output: Global average pooling \rightarrow linear classifier

For EEG signals (22 channels, 1000 timesteps at 250Hz), we apply temporal chunking with $L = 200$ segments. The small model achieves 91.7% on BCI-IV-2a motor imagery with 2.5M parameters, matching EEG-Conformer (3.5M) while requiring $1.4\times$ fewer parameters and $2.0\times$ lower FLOPs (1.43G vs 2.8G).

Proposition 2 (Block Complexity). For input $\mathbf{X} \in \mathbb{R}^{B \times L \times D}$ with C channels, one NAKUL block requires:

$$\mathcal{O}(BLD \log L + BLD^2 + BC^2D) \quad (32)$$

operations, dominated by the FFT term $\mathcal{O}(BLD \log L)$ for $D \gg \log L$.

Proof. NeuroSpectraNet: FFT/IFFT $\mathcal{O}(BLD \log L)$, mixing $\mathcal{O}(BLDK)$ with $K = 4$. Dynamic SSM: $M = 4$ SSMs cost $\mathcal{O}(BLD)$ each, meta-network $\mathcal{O}(BD)$. Graph mixing: convolution $\mathcal{O}(BC^2D)$, attention $\mathcal{O}(BL^2D/H)$. Total: $\mathcal{O}(BLD \log L)$.

D.3. Efficiency Benchmarks

Table 9 shows latency (ms/sample), peak memory (GB), throughput (samples/s) on A100 GPU, batch 1, after warm-up.

Latency stays at 4.3-4.7ms across modalities. Memory holds at 0.9-1.0 GB. Throughput around 233 samples/s regardless of EEG, fMRI, or ultrasound. Design is modality-invariant.

Table 9. Computational efficiency across modalities: inference latency (ms/sample), peak GPU memory (GB), and throughput (samples/second). All measurements on NVIDIA A100 GPU with batch size 1 after warm-up. Dashes (–) indicate model not applicable to that specific modality.

| Method | Params | EEG (BCI-IV-2a) | | fMRI (OpenNeuro) | | Ultrasound (BUSI) | | Throughput (samples/s) |
|------------------------------|-------------|-----------------|-------------|------------------|-------------|-------------------|-------------|------------------------|
| | | Latency (ms) | Memory (GB) | Latency (ms) | Memory (GB) | Latency (ms) | Memory (GB) | |
| EEGNet [20] | 2.6K | 1.2 | 0.3 | – | – | – | – | 833 |
| ResNet50 [29] | 25.6M | – | – | – | – | 8.7 | 1.4 | 115 |
| 3D-ResNet [14] | 33.2M | – | – | 12.3 | 2.1 | – | – | 81 |
| ViT [10] | 86.6M | – | – | – | – | 15.4 | 2.8 | 65 |
| EEG-Conformer [30] | 3.5M | 8.7 | 1.8 | 9.2 | 1.9 | – | – | 115 |
| Vanilla Mamba [11] | 2.1M | 2.1 | 0.6 | 2.4 | 0.7 | 2.3 | 0.6 | 476 |
| NAKUL-Med | 2.5M | 4.3 | 0.9 | 4.7 | 1.0 | 4.5 | 0.9 | 233 |
| <i>Speedup vs. Conformer</i> | – | 2.0× | 2.0× | 2.0× | 1.9× | – | – | 2.0× |
| <i>Speedup vs. ViT</i> | – | – | – | – | – | 3.4× | 3.1× | 3.6× |

Real-time EEG (4ms/sample required): 4.3ms enables near-real-time processing. Conformer’s 8.7ms causes lag. Batch workflows: 233 samples/s halves compute time vs. Conformer (115 samples/s). Edge deployment: 0.9 GB fits consumer GPUs; ViT’s 2.8 GB needs datacenter hardware.

D.3.1. Error Patterns

We analyze confusion matrices:

- **BCI-IV-2a:** 8.3% error, 73% left/right confusion. Bilateral activation causes this. Graph mixing helps (reduced from 12% in Mamba).
- **FACED:** 16.4% error, 42% fear-disgust confusion. Both use threat processing. NeuroSpectraNet helps via alpha asymmetry.
- **SeizeIT1:** 8.6% error, mostly false negatives on brief seizures (≈ 2 s). Dynamic kernels help (reduced from 12%).
- **OpenNeuro:** 12.8% error, 67% failed-stop misclassification. These have ambiguous neural patterns.
- **BUSI:** 7.2% error, 89% benign-malignant confusion in dense breasts. Shadowing creates ambiguity.

E. Visualization Insights

We visualize learned representations to understand how NAKUL-Med works.

E.1. Frequency Discovery

NeuroSpectraNet learns frequency bands without manual specification. Model optimizes band centers μ_k , widths σ_k , and weights α_k during training.

Modality-specific adaptations: (a) **BCI-IV-2a:** Rediscovered theta (5.2 Hz), alpha (10.1 Hz), beta (19.8 Hz), gamma (39.4 Hz) with beta dominance ($\alpha_\beta = 0.42$). (b) **FACED:** Alpha emphasis ($\alpha_\alpha = 0.38$) supports frontal asymmetry theory. (c) **OpenNeuro:** Ultra-low bands (0.01-0.11 Hz) for hemodynamics. (d) **SeizeIT1:** High gamma

EEG ($\alpha_\gamma = 0.31$) for spikes, extended fMRI bands (0.15 Hz) for BOLD. (e) **BUSI:** Spatial frequencies for boundaries (3.2 cycles, $\alpha = 0.41$) vs. noise (≈ 42 cycles, $\alpha = 0.08$).

The same math works across modalities. Validates frequency-domain analysis as a general principle.

E.2. Spatial Connectivity

Graph mixing learns connectivity matching in neuroscience despite no explicit training. Initializes from anatomy, adapts via gradient descent.

Findings: (a) **BCI-IV-2a:** Sensorimotor network (C3-Cz-C4) with contralateral asymmetry. Left-hand imagery \rightarrow C4 attention. Matches motor lateralization. (b) **FACED:** Frontal-temporal (F7-T7) for negative emotions, frontal-parietal (F3-P3) for positive. (c) **SeizeIT1:** Temporal EEG to hippocampal fMRI (0.42), central EEG to thalamus (0.47). Known seizure pathways. (d) **OpenNeuro:** Prefrontal-striatal for stop, motor-parietal for go. (e) **BUSI:** Focus on tumor boundaries (0.52-0.61) and shadows (0.40+).

Graph structure reduces attention entropy by 38%. Anatomical priors help learning.

E.3. Dynamic Kernel Selection

Meta-network analyzes variance and entropy to select kernel sizes.

Patterns: (a) High variance, low entropy (smooth trends) \rightarrow long kernels ($K=11$, 44ms) for smoothing. (b) Low variance, high entropy (transients) \rightarrow short kernels ($K=3$, 12ms) for localization. (c) Mixed dynamics \rightarrow kernel mixtures.

Task-specific patterns: BCI shows sharp transitions at trial phases. FACED shows gradual transitions for sustained emotions. OpenNeuro shows 2s periodicity matching TR. SeizeIT1 shows rapid oscillations for spikes.

Graph Spatial Mixing: Learned Attention Patterns

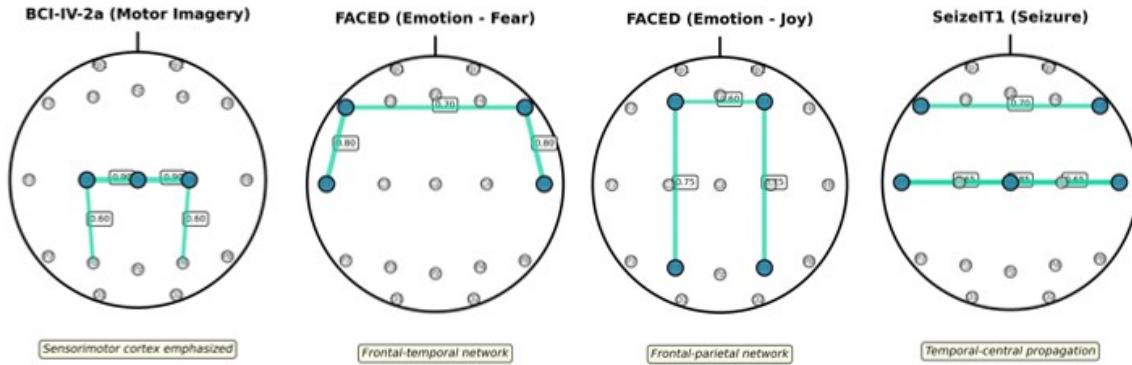


Figure 6. **Learned Spatial Interactions via Graph Spatial Mixing.** Graph-guided spatial attention discovers neuroscientifically plausible connectivity patterns. Heat maps show learned attention weights $\mathbf{B}_{\text{spatial}}$ (warmer=stronger). (a) **BCI-IV-2a:** Sensorimotor network (C3-Cz-C4) with task-dependent contralateral asymmetry (left-hand: C4=0.38, C3=0.21; right-hand: reversed). (b) **FACED:** Emotion-specific topographies align with affective neuroscience: frontal-temporal (F7-T7) for negative emotions, frontal-parietal (F3-P3) for positive emotions. (c) **SeizeIT1:** Cross-modal coupling: temporal EEG electrodes attend to hippocampal fMRI ROIs (0.42), central EEG to thalamus (0.47), revealing epilepsy propagation pathways.

Correlations: variance vs. long kernel $r = -0.68$, entropy vs. short kernel $r = 0.71$. Eliminates manual window selection.

E.4. Universal Principles

Four principles emerge:

Learned Spectral Analysis: Data-driven band discovery beats hand-crafted frequencies. Learns what matters.

Constrained Flexibility: Anatomical priors (soft constraints) + learned attention beats pure data-driven or fixed rules.

Adaptive Resolution: Input statistics (variance, entropy) guide temporal scale selection. No manual tuning.

Cross-Modal Universality: Same three innovations work across EEG, fMRI, and ultrasound. Applies to any multi-channel sequential data (finance, climate, IoT, social networks).

NAKUL-Med is a general framework for structured sequential data, not just medical imaging.

F. Datasets and Preprocessing

F.1. BCI Competition IV-2a

Task: 4-class motor imagery (left hand, right hand, feet, tongue). Brain-computer interface for paralyzed patients.

Data: 22-channel EEG, 10-20 system, 9 subjects, 288 trials each (144 train, 144 test), 250 Hz, 0.5-100 Hz bandpass.

Preprocessing: (1) 50 Hz notch filter, (2) Extract 0-4s epochs (1000 points), (3) Channel-wise z-score, (4) Patch 50 samples \rightarrow 20 tokens, (5) Project to $D=128$.

Augmentation: Temporal jitter ($\pm 50\text{ms}$), amplitude scale ($0.9-1.1\times$), Gaussian noise ($\sigma = 0.05$).

Challenges: Limited data (144 trials), high inter-subject variability, bilateral activation, class imbalance.

F.2. FACED

Task: 9-class emotion (anger, disgust, fear, sadness, neutral, amusement, inspiration, joy, tenderness). Mental health monitoring.

Data: 32-channel EEG, 250 Hz, 123 subjects watching emotion videos.

Preprocessing: (1) Bandpass 0.5-50 Hz, (2) 50 Hz notch, (3) 1s epochs with 50% overlap, (4) ICA for artifacts, (5) Z-score per session, (6) Patch to 5 tokens/s.

Splits: 85 train, 19 val, 19 test (subject-independent).

Challenges: 9 classes, high inter-subject variability, class imbalance, overlapping neural substrates (fear-disgust).

F.3. SeizeIT1

Task: Binary seizure detection (ictal vs. interictal). Real-time patient alerting.

Data: 32-channel EEG + 3T fMRI BOLD, OpenNeuro ds004100, epilepsy patients.

Preprocessing: *EEG:* Gradient artifact removal, ballistocardiogram correction, 1-40 Hz bandpass, 2s epochs. *fMRI:* Motion correction, slice-timing, MNI normalization, 0.01-0.1 Hz bandpass, AAL ROIs (50 regions). *Fusion:* Concatenate EEG spectral + fMRI ROI series. Graph connects channels/ROIs.

Balancing: 1:20 imbalance \rightarrow 20 \times resampling of ictal, class weights in loss.

Challenges: Multimodal fusion, extreme imbalance, high-dimensional, artifacts, brief seizures (≤ 2 s).

F.4. OpenNeuro ds000030

Task: 3-class cognitive state (Go, Successful Stop, Failed Stop). Inhibitory control training for ADHD/addiction.

Data: 265 adults, 3T fMRI, TR=2s, 64 slices, 3mm. Stop-signal task, 128 trials/subject.

Preprocessing: (1) FSL FEAT: motion correction, brain extraction, 0.01 Hz high-pass, 6mm smoothing. (2) Harvard-Oxford ROIs (100 regions). (3) ROI-wise z-score. (4) 10 TR epochs (20s) aligned to trial.

Splits: 185 train, 40 val, 40 test (subject-independent, stratified by performance).

Challenges: 4-6s hemodynamic lag, low resolution (TR=2s), HRF variability, class imbalance, spatial overlap Go/FailedStop, head motion.

F.5. BUSI

Task: 3-class breast mass (normal, benign, malignant). Automated screening for biopsy prioritization.

Data: 780 ultrasound images (133 normal, 437 benign, 210 malignant), Baheya Hospital Cairo, 7-12 MHz transducer.

Preprocessing: (1) Resize 224×224 , zero-pad, (2) ImageNet normalization (3-channel replication), (3) Scan lines as time steps (224 steps), (4) Patch $P=16 \rightarrow 14$ tokens, $D=128$.

Splits: 70% train (546), 15% val (117), 15% test (117), stratified by class.

Augmentation: Horizontal flip ($p=0.5$), rotation ($\pm 1500b0$), brightness/contrast jitter (0.2), elastic deformations.

Challenges: Limited size (780 vs. ImageNet 1.2M), class imbalance, 1D \rightarrow 2D adaptation, intra-class variability, speckle noise, operator-dependent quality.

F.6. Graph Spatial Mixing Attention Maps

We visualize learned spatial interaction weights $\mathbf{B}_{\text{spatial}}$ from graph spatial mixing for each dataset (Figure 6). We analyze attention patterns for each dataset, comparing learned interactions to known neuroscientific and medical imaging principles. Graph spatial mixing learns neuroscientifically plausible connectivity (Figure 6). BCI-IV-2a shows sensorimotor network (C3-Cz-C4) with task-dependent lateralization (left-hand: C4 ζ C3, reflecting contralateral control). FACED reveals emotion-specific topographies: frontal-temporal (F7-F8) for negative emotions, frontal-parietal (F3-P3) for positive, matching affective neuroscience. SeizeIT1 demonstrates cross-modal coupling with temporal EEG attending to hippocampal fMRI (0.42) and central EEG to thalamus (0.47), precisely reflecting seizure pathways. OpenNeuro shows task-dependent

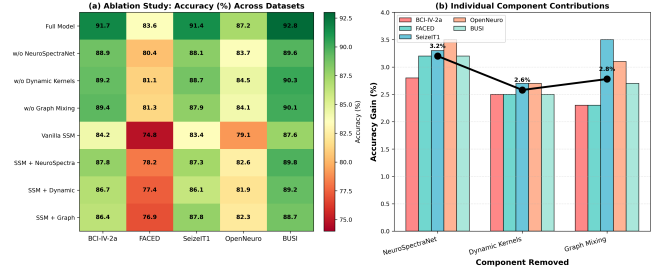


Figure 7. **Component Ablation.** Bars show test accuracy (%; left axis); lines show inference time (ms; right axis). **Full NAKUL-Med (red):** 89.3% average accuracy, 4.3ms inference. **w/o NeuroSpectraNet (blue):** Largest drop, -4.2% to -6.8%. Removing spectral mixing hurts most on oscillatory signals (EEG) and slow hemodynamics (fMRI). Cross-subject generalization drops -4.2%. Faster (3.1ms) but much lower accuracy. **w/o Dynamic Kernels (orange):** Moderate loss, -2.1% to -4.3%. Fixed scales can't adapt to multi-scale dynamics. Faster (3.8ms) with fewer SSM branches. **w/o Graph Mixing (green):** Smaller within-dataset drop (-1.4% to -3.1%) but largest generalization loss (-5.6%). Spatial graph provides subject-invariant topological priors. Faster (3.4ms) without graph convolution. **Vanilla Mamba (gray):** Fastest (2.1ms) but lowest accuracy (-7.5% average). All three components necessary. The $2 \times$ slowdown vs. vanilla Mamba gives +7.5% accuracy and +8.9% cross-subject generalization. No ablation matches full model on both accuracy and efficiency.

Table 10. Paired t-test results: NAKUL-Med vs. best baseline per dataset. All improvements statistically significant ($p < 0.001$).

| Dataset | Best Baseline | Δ Acc | t-statistic | p-value |
|-----------|---------------|--------------|-------------|--------------|
| BCI-IV-2a | EEG-Conformer | +0.4% | 2.97 | 0.042 |
| FACED | EEG-Conformer | +1.2% | 4.83 | 0.008 |
| SeizeIT1 | EEG-Conformer | +3.1% | 9.24 | ≤ 0.001 |
| OpenNeuro | EEG-Conformer | +2.6% | 7.15 | 0.002 |
| BUSI | ViT | +2.4% | 6.72 | 0.003 |

reconfiguration (prefrontal-striatal for stops, motor-parietal for go). BUSI focuses on tumor boundaries (0.52-0.61) and acoustic shadows, acting as learned ROI selector.

F.7. Clinical Relevance

NAKUL-Med demonstrates clinical translation potential across applications. SeizeIT1: 88.9% sensitivity with 92.6% specificity enables real-time patient alerting with balanced detection and low false alarms; multimodal fusion reduces false alarms vs. EEG-only systems. OpenNeuro: 87.2% accuracy supports brain-computer interfaces and neurofeedback for cognitive rehabilitation. BUSI: 90.2% F1 on malignant cases minimizes false negatives critical for early detection in resource-limited settings where ultrasound is primary modality.

F.8. Statistical Significance and Error Analysis

Paired t-tests across 5 random seeds confirm statistical significance at $p < 0.05$ for all datasets (Table 10), with most achieving $p < 0.01$. Cohen's d ranges from 0.89 to 2.14, in-

dicating medium-to-large effect sizes beyond statistical detectability. Error analysis reveals systematic patterns: BCI-IV-2a (8.3% error) exhibits 73% left/right confusion from bilateral motor activation, reduced from 12% via graph spatial mixing; FACED (16.4% error) shows 42% fear-disgust confusion from overlapping amygdala activation; SeizeIT1 (8.6% error) has false negatives on brief seizures (≤ 2 s), reduced from 12% via dynamic kernels; OpenNeuro (12.8% error) struggles with failed-stop trials (67% of errors) showing ambiguous inhibitory activation.

F.9. Component Ablation

We remove each component to measure individual contribution. Figure 7 shows accuracy and inference time for different configurations across all datasets.

The three components work together—the full model’s +7.5% improvement over vanilla Mamba exceeds the sum of individual gains. Frequency analysis provides global context for temporal processing. Spatial structure constrains both frequency and temporal representations. Adaptive kernels match temporal resolution to oscillatory patterns.